Development of a Novel Sensor For Soil Moisture's Profile

by

Toan Canh Nguyen

Presented to the Faculty of the Graduate School of

The University of Texas at Arlington in Partial Fulfillment

of the Requirement

for the Degree off

MASTER OF SCIENCE IN ELECTRICAL ENGINEERING

Department of Electrical Engineering

University of Texas at Arlington

May 2022

Acknowledgements

I would like to express my gratitude to my advisor, Dr. Tjuatja. His guidance and support have helped me tremendously through this journey. I would like to extend my gratitude to my commitee's members, Dr. Xinbao Yu and Dr. Jonathan Bredow for their time and constructive feedback to my work.

I would like to thank my parents, Tao Nguyen and Trang Nguyen, and my aunt, Hau Nguyen, for their unconditional love and support. They have sacrificed their lives for my education. I would like to express my gratitude to my brother, Khoa Nguyen and especially my sister, Hoa Nguyen, for everything they have done to help me. Thanks to them, I have the privilege of finishing my study debt-free.

I would like to express my gratitude to my mom's extended family. They have raised and guided me ever since I came to America. They never turn their back against me and always welcome me back regardless of how mistakes I have made. I am grateful to be born in this loving and supportive family.

Abstract

Monitoring of soil's water content has been an important part of the irrigation system in farming, regional resources development, rainfall detection as well as disaster prevention. There has been studies and developments in this area over the decades. However, most of the works are focused on sensing the soil as a homogeneous medium, which does not accurately reflect the heterogeneous structure of soil. Works on multi-layer soil sensing have been researched and developed. Though, the current design is complex, not easy to produce and assemble. This work presents a novel low-cost and simple soil sensor design to detect the soil's water content at different layers. The design is capacitive approach. In this method, soil acts as the medium whose dielectric values vary with its water content. These changes result in shifts in resonant frequencies of the sensor's structure, which can be used to determine the water content of the soil. This sensing approach is simple, inexpensive, easy to set up and portable. For soil profile sensing purposes, the soil depth's information is encoded in the sensor's physical structure. Instead of using a rectangular plate, the sensor's shape is varied exponentially. As the capacitive effect depends on the area of the conductor, this design allows for more changes in soil profile to be captured. A theoretical model for this sensor design was developed with Transmission Line and ABCD Network in MATLAB. A similar model was set up in High-Frequency Simulation Software (HFSS) for comparison. The deign was tested in medium which consists of two different soil profiles. The boundary between the two profiles varied along the length of the sensor. The results in theoretical and simulating model showed corresponding changes in resonant frequencies as the soil boundary changes in three different cases. A lab measurement was arranged to compare the performance of this proposed design (exponential shape) with the standard one (rectangular shape). This setup was also modeled in simulating software for comparison. The results showed that proposed sensor design had higher sensitivity

when the boundary layer varied toward end of the sensor. Finally, the effect of the proposed sensor design's parameter was studied in HFSS and the design for the sensor was finalized to achieve the highest sensitivity.

Contents

List of Figures

Chapter 1

Introduction

1.1 Overview

Food and water are the two most important resources on which our society depends. With increasingly severe climate change and overpopulation, there is a need to develop a more efficient and productive agricultural system. For this purpose, water-content sensing of soil is the focus. It provides information on what's going inside the ground. The irrigation system can then make more accurate and efficient decision (1.1).

Figure 1.1: Irrigation system

Soil sensing is not limited to that area. Soil sensor can potentially be used to measure the moisture level of other medium such road or bridges. This is an important application, especially during the winter. Icy condition is sometimes not visible to human eyes. With soil sensor employed, the condition of the road can be determined. Better decision can be made and many lives could potentially be saved (1.2).

Majority of the development of soil sensing focus on treating soil as homogeneous medium. This does not reflect the inhomogeneous nature of soil. Works on profile soil sensing have been studied and presented over the year. However, the design is complex and inflexible. This work presents a novel simple design for soil profile sensing. The sensor is designed to detect changes in soil boundary layer.

This paper is organized in following order: Overview of the current soil

Figure 1.2: Icy bridge in the winter

sensing techniques, introduction of the novel sensor for soil's moisture profile followed by the performance and parametric analysis of the proposed design.

1.2 Direct Measurement - Gravimetric Method

Soil water content can be measured directly with gravimetric method. In this approach, the water content of the soil is obtained by determining the weight difference between the initial soil sample and after it dries out [8]. After the soil sample is to be carefully taken and initially weighted, the sample is then carefully dried. Then the sample would be weighted again. The ratio between the difference in weighs and the dry soil is the water content of the soil (Fig.1.2.1). While accurate, it is time- and labor-consuming. This method requires decent amount of time to execute (Fig.1.3. When the result arrives, it could potentially be no longer accurate as the soil content might have changed. Thus, gravimetric method is hard to scale for continuously monitoring of soil conditions.

$$WaterContent = \frac{m_{wet} - m_{dry}}{m_{dry}} \tag{1.2.1}$$

Alternatively, there are other ways to determine water content of the soil indirectly. With these approaches, the amount of water inside the soil can be obtained through other measurements soil's characteristics. Those measurements depends on

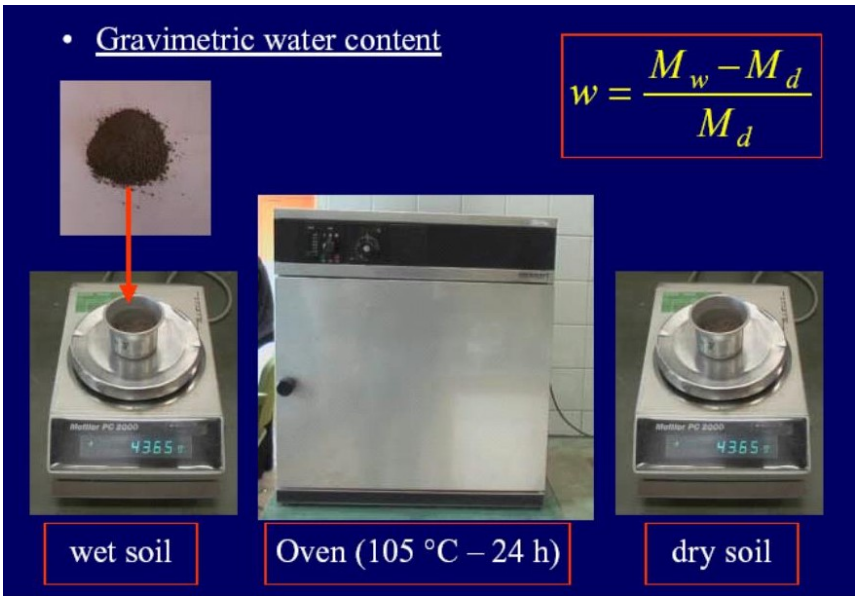

Figure 1.3: Direct measurement to determine gravimetric water content of the soil

the water content of the soil. Their effectiveness are determined by factors such as cost, accuracy or maintenance. The most common category of Indirect Measurement is in-situ sensor.

1.3 Indirect Measurement - In-situ Sensor

In-situ sensing is a non-destructive sensing method as the sensing equipment is buried and stay within the ground. Measurements can be designed to be taken at anytime and at variable depths. In-situ sensing relies on various soil's properties which are affected by the amount of water content. In this paper, we are reviewing sensing approaches based on water potential, thermal property and electrical properties of soil.

1.3.1 Soil Water Potential - Tensiometer

In this method, the sensor is designed to behave like a plant's root. It measures how water being absorbed by the plant. This sensor consists of distilled water contained in a tube, a porous tip at the bottom and a pressure gauge (Fig.1.4). In presence of water potential difference between the tub and the soil surrounding

it, water would be moving accordingly [9]. For example, when water potential difference favors the tub, the water inside the sensor would try to move into the dry soil through the porous tip and vice versa. This will create a tension which can be measured by the pressure gauge. Since it is proportional to the medium's moisture level, this information can be used to determine the amount of water available within the soil [10]. In other word, the water level of the soil is measured indirectly through the recorded pressure created by water moving through the porous tip.

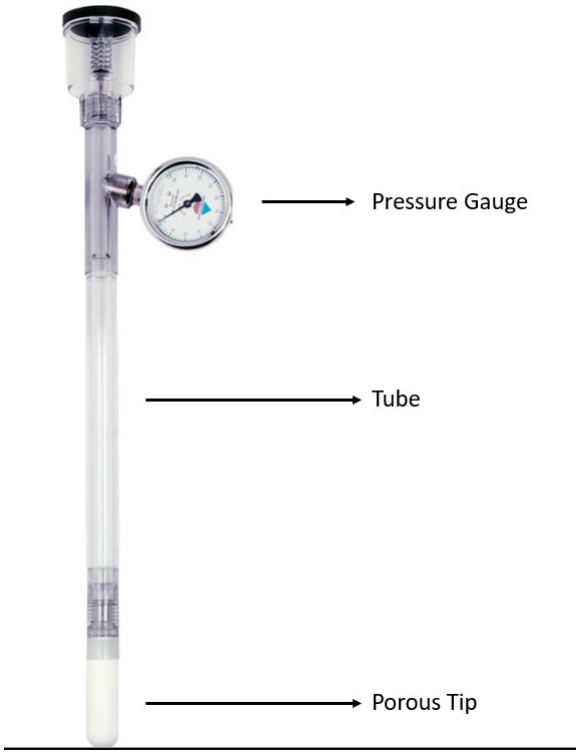

Figure 1.4: General structure of tensiometer

This process is independent of soil's type and temperature. However, since the measurement relies on the movement of water between the sensor and soil, tensiometer can't be used in freezing condition as water's movement is restricted which effectively hinders the accuracy of the reading.

1.3.2 Thermal Properties - Thermal heat probe

The amount of water within the soil directly affects the its thermal conductivity. This property depends on the amount of water within the medium and can be

indirectly measured by its ability to dissipate heat. Thus, the soil water content can be derived from the measurement of a temperature sensor. A thermal probe sensor generally consists of a thermal sensor and a thermal source (Fig.1.5). The thermal source release a heat pulse and the thermal sensor measure the heat dissipation of the medium. Variations of the thermal heat probe sensor has been presented in literature. There is a design which consist of one single probe as both thermal source and thermal sensor can be packed into it. This design is low-profile and suitable for small environment applications [11]. On the other side, the multiple-probe sensor offers higher sensitivity when the application allows for more sizable equipment. In this case, the thermal sensor and the thermal are two separate components [12].

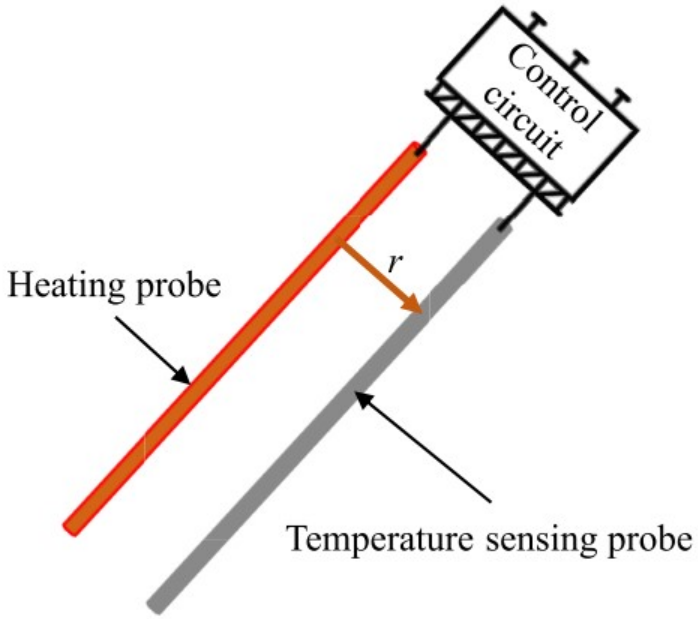

Figure 1.5: General diagram of a thermal heat probe sensor [1]

Thermal heat probe is a cost-effective sensing method. Since it relies on the thermal property of the soil, this approach is independent of soil's type and salinity. However, this method requires more energy (compared to other methods) and is prone to error due to ambient temperature and changes in humidity

1.3.3 Neutron Moderation - Neutron Probe

Neutron moderation sensor consists of two main components, a probe containing the radioactive neutron source with fast neurons and a detector connected through a cable (Fig.1.6). Upon released, the fast neurons would collide with atoms in soil and slow down depends on the collision effects. This effect is higher with low atomic weight atom than the heavy one. Since hydrogen is the only light weight atoms found in significant amount in soil, this method can be used to determine the water content of a medium. When the fast neurons slow down after the collision with hydro atoms, they form a cloud slowed atoms [13]. If the soil is dry, the atoms released from the probe would be able to travel further without many collisions. Thus, the cloud of slowed atoms would be less dense. In the opposite case, with wet soil, the cloud of slow atoms around the probe would be denser. The sensor in the gauge is designed to ignore the fast atoms and only count the slow one. Thus, measurement of slowed-atom cloud's density can be used to determine the water content of the soil.

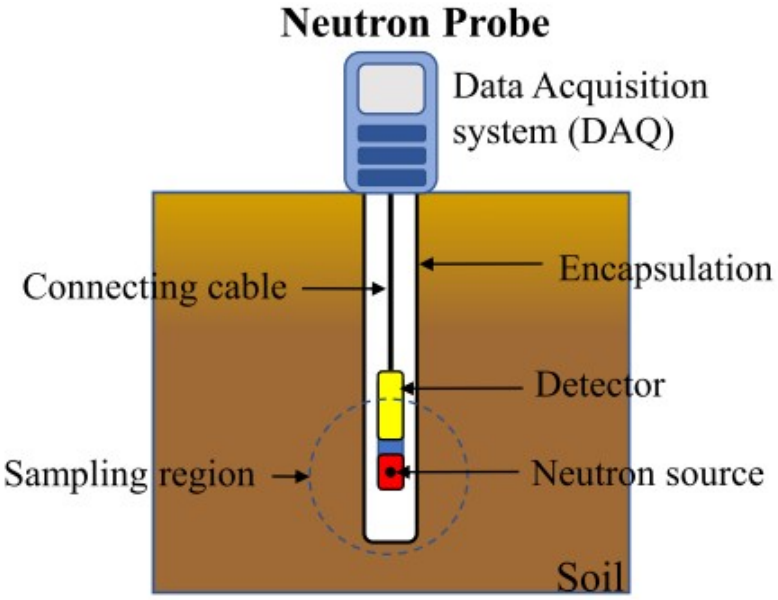

Figure 1.6: General Diagram of a measurement setup for Neutron Probe [1]

Neutron moderation probe is a robust and reliable method for soil sensing.

This approach measures water content of soil by considering the collision the between the radioactive fast neutron contains inside the probe and soil's hydrogen atoms. Thus the measurement is independent of the medium's salinity or air gaps. On the other hands, this soil sensing approach does come with some disadvantages. Since neutron probe's working principle is around radioactive atoms, safety hazard has to be considered. For the similar reason, this device is expensive to acquire.

1.3.4 Electrical Properties - Dielectric permittivity

Dielectric parameter of soil

In electromagnetism, dielectric are the materials which have poor conductivity and capable of store electrical charge due to dielectric polarization. When a dielectric is placed in an electrical field, its atoms are shifted slightly from their equilibrium position. The positive charges align with the field while the negative one are against it (1.7). This results in an internal electrical field. It is the working principle of capacitor and how it stores energy [14].

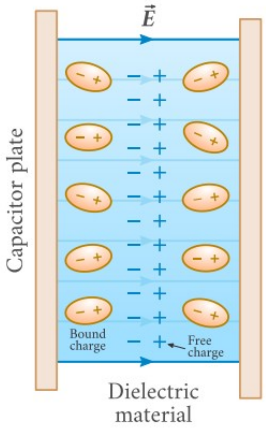

Figure 1.7: Dielectric Polarization

Electric polarizability of a material is often expressed in term of relative permittivity or dielectric constant ϵ_r. Dielectric constant of a material is the ratio of its electrical permittivity over the vacuum's ϵ_o (Eq.1.3.1). This parameter highly depends on the water content of a medium. For example, the dielectric constant

of a dry soil is around 3 to 5. For water, it is 80 [8]. Thus, soil moisture can be determined through the measurement of its dielectric constant value.

$$\epsilon_r = \frac{\epsilon}{\epsilon_o} \tag{1.3.1}$$

Time-domain Approach

As mentioned above, the amount of water inside the soil is directly proportional to its dielectric constant. As we would discuss in the next chapter, the velocity of an electromagnetic waves travelling within a medium depends on its dielectric constant. Higher dielectric constant means slower velocity. Thus, by measuring the traveling time of wave, the dielectric value soil can be obtained [14].

Time-domain reflectometry is the sensing technique following this concept. It has been used to detect faults on the wire since 1930s and was then used in soil sensing [15]. The setup for this approach usually consists of pulse generator capable of producing precisely timed electrical pulse, an oscilloscope to observe the reflected signal and a pair of (or multiple) conductors (Fig.1.8).

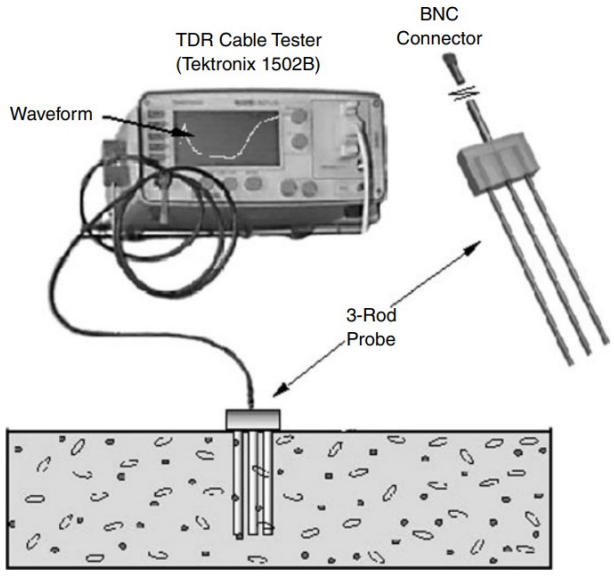

Figure 1.8: General setup of a Time-Domain Reflectometry soil sensor (3-probe) [2]

When the generator sends out the electrical pulse, it would be transmitted to the probes through coaxial cable. Due to impedance mismatching (between the

probe and the cable), part of the signal would be reflected back to the source. This reflection is recorded by the oscilloscope and referred as the first reflection point. From there. the pulse travels down the probes. At the end of the line, upon a discontinuity, the signal would be reflected back to the source. The reflection is recorded by the oscilloscope and referred as second reflection point [3]. The time difference between the two reflection points is the time it takes the electrical signal travel the probes twice (Fig.1.9). As the medium surrounding the conductor affect the velocity of the signal, knowing the probe's length, the dielectric constant value of the soil can be determined (Eq.1.3.2). ϵ_r is the dielectric constant. t is the traveling time and L is the length of the probe.

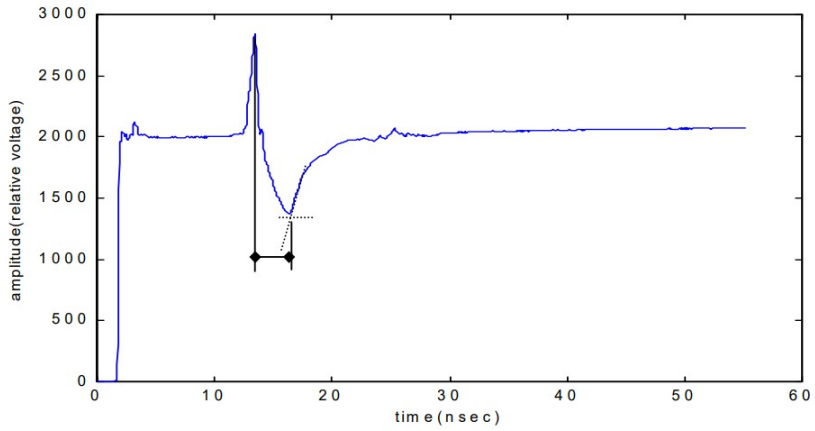

Figure 1.9: Reading of TDR sensor [3]

$$\epsilon_r = (\frac{ct}{2L})^2 \tag{1.3.2}$$

Time-domain reflectometry is a reliable soil sensing method. The probes' design is simple and flexible. It does not create disturbances in the soil upon insertion. The sensor can also be modified to also measure the quantities such as thermal conductivity, thermal diffusivity, volumetric heat capacity [4](Fig.1.10).

However, this method comes with some drawbacks. TDR measures the soil's water content through the traveling time of the electrical signal. Since measurement in time-domain is short (10-15ps), a sophisticated analysis system is needed. Thus, this approach is not affordable. Another disadvantage of TDR system is that it

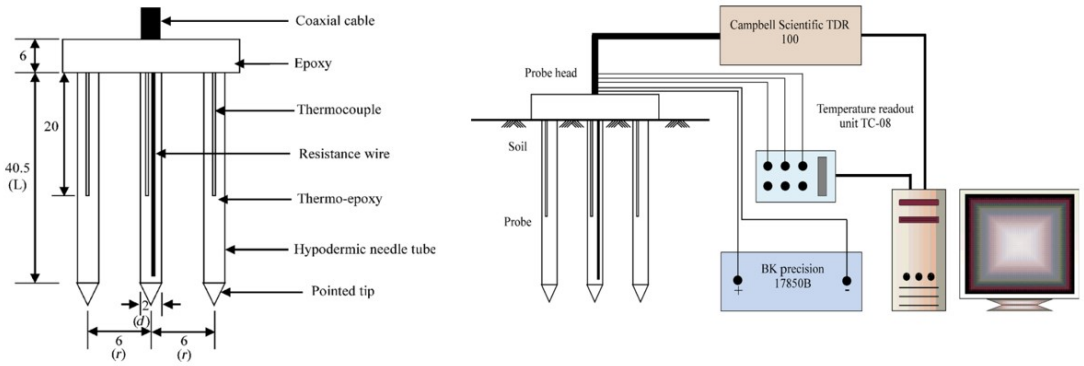

Figure 1.10: Schematic and setup of a modified TDR sensor for other measurements [4]

is not suited to measure in-homogeneous mediums. As we will discuss in the next chapter, electromagnetic waves would be reflected upon any discontinuities. It could be the end of the line or simply changes in soil medium, which causes changes in the line's impedance. Thus, with more than one reflection, the reading could be noisy and affects the accuracy of the results (Fig.1.11).

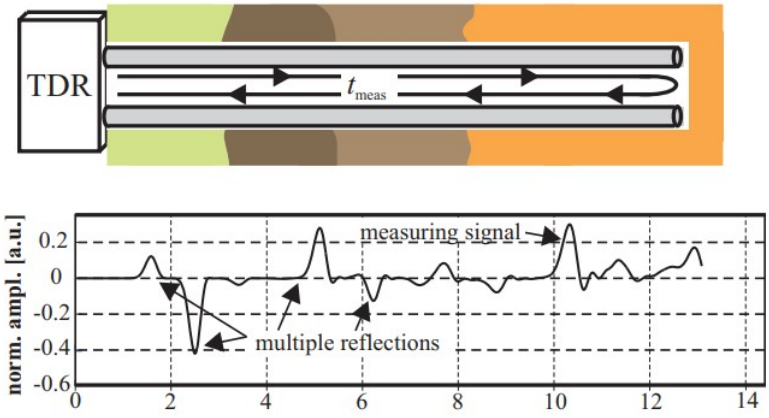

Figure 1.11: TDR measurement with multiple reflections [5]

Time-Domain Transmission (TDT) is another approach which relies on the same working principle as TDR. However, TDT is designed to not be affected by the above-mentioned multiple reflections problem. TDT is fundamentally similar to TDR. An electrical wave is generated from a signal generator travels along probes whose length is known. The traveling time is recorded and used to determine the

soil's moisture content. The difference between them is that instead of having open-circuit design, TDT has closed-loop design for its probes (Fig.1.12). TDT is interested in the time it takes the electrical signal to travel around a closed-loop probe design. It does not take in consideration of any reflections happen along the way. When the voltage threshold is crossed at the other end of the probe, the time is recorded . As a result, TDT is not affected by multiple reflections. This advantage makes TDT is better suited for measurement in-homogeneous soil. However, since the design is closed-loop, compared to TDR, it is harder to insert TDT probe into the soil without causing disturbances.

Figure 1.12: Different probes design for TDT sensing method [5]

Capacitance Approach

As discussed above, dielectric constant of a medium is proportional to its water content. Dielectric value of wet soil is high and in the case of dry soil, it is low. Dielectric constant of a medium is a complex value (1.3.3). However, dielectric constant is usually expressed in term of its real part and loss tangent (**??**). Loss tangent is the tangent of the angle between the field vector and the loss component. In other word, the higher loss tangent, the higher losses of energy in the medium. This is usually the case for wet soil.

$$\epsilon = \epsilon_r + j\epsilon_i \tag{1.3.3}$$

Medium	Dielectric Constant	
	Real	Loss Tangent
Dry Soil	3	0
Wet Soil (20%)	8-10	0.232
Water	80	0.005-0.16

Figure 1.13: Dielectric values of soil and water

$$tan\delta = \frac{-\epsilon_i}{\epsilon_r} \tag{1.3.4}$$

Electrical permittivity is a factor deciding the medium's capacitive effect [14]. In Eq.1.3.5), capacitance is proportional to the dielectric constant of the medium, the surface area of conductor and inversely proportional to the distance between the two conductor. With that in mind, it is possible that measured capacitance can be used to determine the soil water content. This is the sensing approach of capacitance sensor.

$$C = \frac{\epsilon_o \epsilon_r A}{d} \tag{1.3.5}$$

When an voltage source is applied to a RC circuit, the capacitor C would start charging up. Over the time, the voltage across that capacitor would rise as charges are accumulating on the capacitor's terminals. How fast the voltage rises depends on the resistor R and capacitor C. Thus, by determining the rise time, the soil's water content can be derived.

Figure 1.14: Commercial Capacitive soil sensor [6]

On the same approach, the resonant frequency of a circuit depends on its capacitive values (Eq.1.3.6). Different medium would result in different resonant frequencies. Thus, soil's water content can be determined through that measurement. This is the working principle of capacitance and Frequency-Domain Reflectometry (FDR) sensing technique.

$$f_o = \frac{1}{2\pi\sqrt{LC}} \tag{1.3.6}$$

FDR sensor usually consists of a probes acting as capacitor and an oscilloscope. In RLC circuit, the resonant frequency is the inverse of the square root of inductance multiplied with capacitance (Eq.1.3.6). Assuming the inductance is constant, the resonant frequencies would be shifted to the lower band in the cases of higher capacitance and vice versa. In FDR sensor, the oscillator's frequencies are swept within a certain frequency band. The one at which results in highest amplitude is the resonant frequency of the RC circuit. Changes in this measurement is corresponding to the changes in water content of the medium [16] (Fig.1.15). In some cases, the oscillator can be replaced with a Vector Network Analyzer (VNA) instead to record the shift in resonant frequencies.

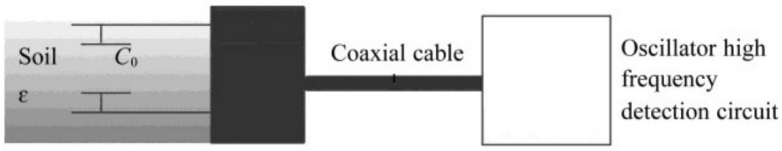

Figure 1.15: Simplified diagram of a FDR sensor [7]

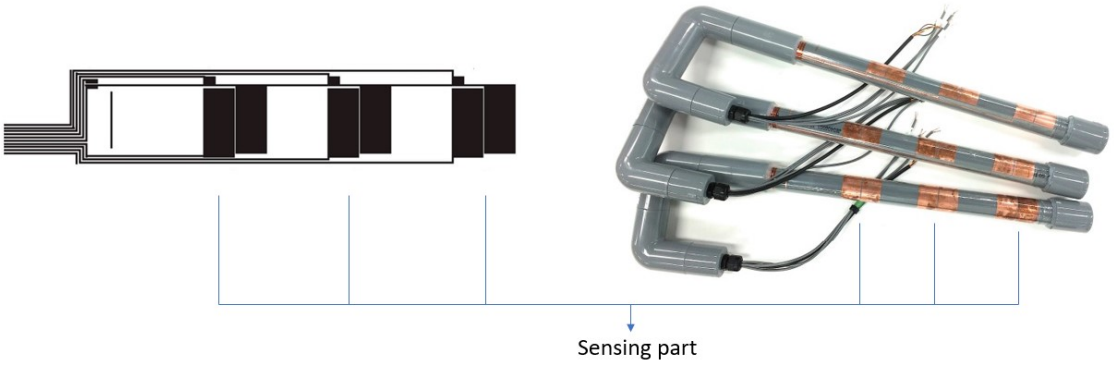

Figure 1.16: Diagram of the the soil profile sensor designed by Kojima et al

1.3.5 Proposed Sensor Design

Most of the researches about soil sensing treat soil as a homogeneous medium. This does not accurately reflect the heterogeneous nature of the soil. For example, with water tend to move down, the top layer is usually drier than the lower ones. Precise information about the water content of soil at different depth is crucial, especially in agriculture as the root zone is usually quite deep (about 50cm).

Some works has been done for soil profile sensing. Kojima et al. [17] designed a profile sensor which employs three different capacitance sensor at three different depth. The sensor have rectangular thin-film capacitors wrapped around a tube. The three capacitor are placed separately at equal distance (Fig.1.16). Similar approach was studied by Zhenran et al. [18] Soil profile sensing was done by annular electrodes at different depths (Fig.1.17). These two studies follows the capacitance approach. Soil moisture content is obtained through the measurement of capacitance.

The two above-mentioned sensors are design to detecting moisture level at specific depth with capacitive approach. However, the depth sensing is predeter-

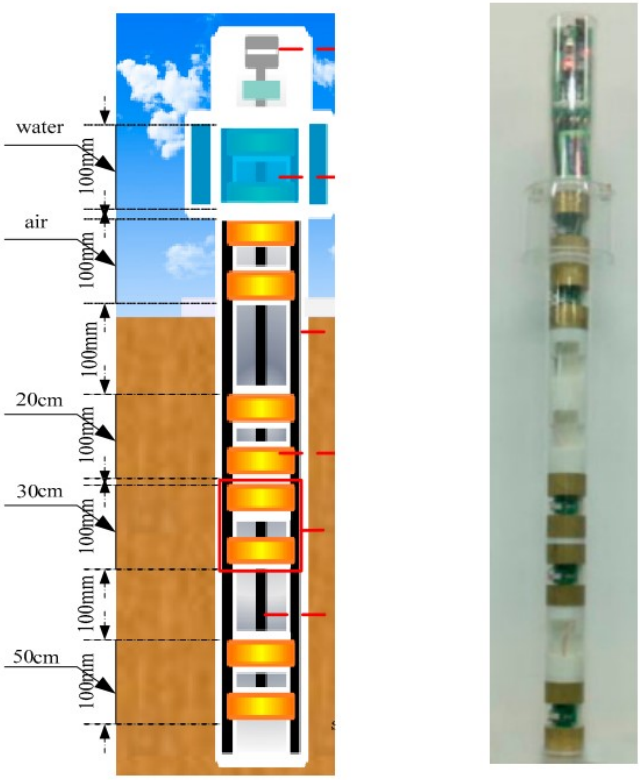

Figure 1.17: Diagram of the the soil profile sensor designed by Zhenran et al

mined and inflexible. Thus, they could potentially misread the soil's conditions due their placements. This work presents a novel sensor design for continuous soil moisture profile sensing. The design follows the capacitance approach, similar to the two above-mentioned studies. However, instead of specifically designate the sensing depths with, the design aimed to encode the continuous depth information to the sensor's physical structure. The proposed sensor design has it shape varied exponentially along the length (Fig.1.18). The width of the sensor is governed by the exponential equation (Eq.1.3.7). l is the length of the sensor. A is the scale constant and α is the attenuation constant. In the context of this study, A and α would be referred as end-width and curvature constant respectively.

$$Width = Ae^{-\alpha l} \tag{1.3.7}$$

As the capacitive effects of the capacitor depends on the the medium between the surface area of the metal probe, the proposed sensor would be able to

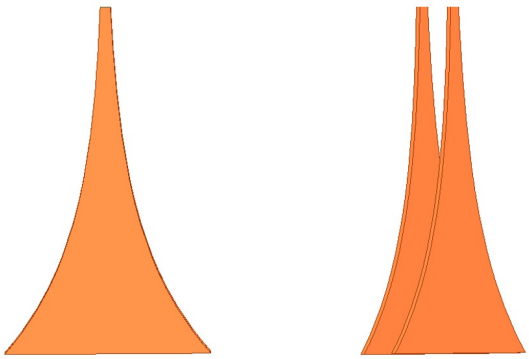

Figure 1.18: Proposed sensor design with exponential shape

capture more changes in soil layers. The measurement is S11 of the S-parameter. It can be measured by Vector Network analyer (VNA). In the next chapter, theoretical and simulating models are made to verify the design's capability.

The aim of this study is to explore the possibility of the new design for soil moisture profile sensing. Lab measurements were done with specialized equipment which are not meant for field uses. This work is an initial step in a working progress of a soil sensor capable of continuous profile sensing.

Chapter 2

Design Verification

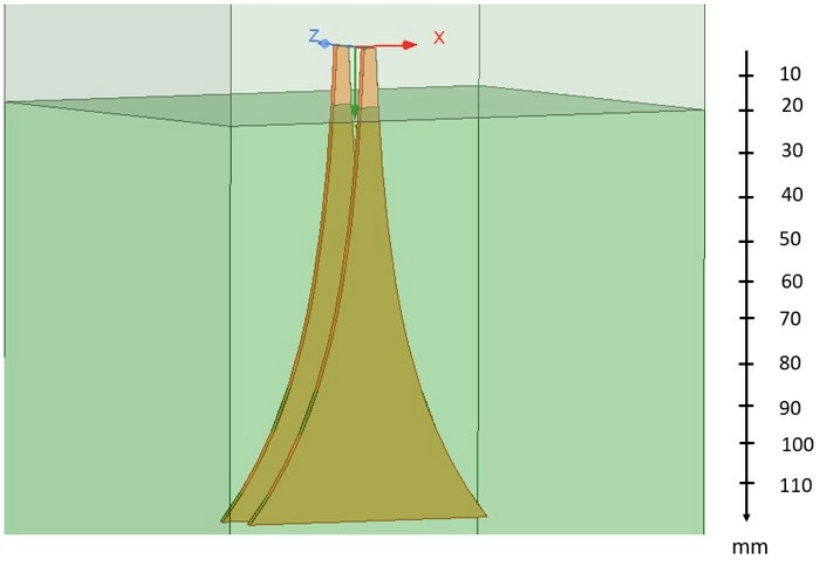

Figure 2.1: Setup for design verification with varying boundary layer

The proposed sensor is designed to detect changes in soil layer boundary (2.1). The sensing capability of the proposed sensor design is verified through its theoretical and simulating model. The testing design is 120mm-long, the distance between two plate is 10mm, the curvature constant α is 0.025 and the end-width is 70mm (Fig.2.2). The theoretical model is developed with transmission line theory and the transmission matrix ABCD. The simulating model is built in the High-frequency structure simulator (HFSS). The test soil is sandy. The dielectric values of sandy soil at different moisture level is obtained from Dr. Ulaby's report [8]. The two model were placed in three different scenarios of soil.

The parameter-of-interest of the proposed sensor design is is the shift in resonant frequencies, which is shown in reflection coefficient S11. S11 represents how much power is reflected back to the source in comparison to the total transmitted power. Resonant frequency is affected by the sensor's structure and its surrounding medium.

- Case 1: Dry soil and 10%-water soil
- Case 2: 10%-water soil and 20%-water soil
- Case 1: Dry soil and 20%-water soil

The result shows that the proposed sensor design is capable of capturing changes as the depth of the soil layers change.

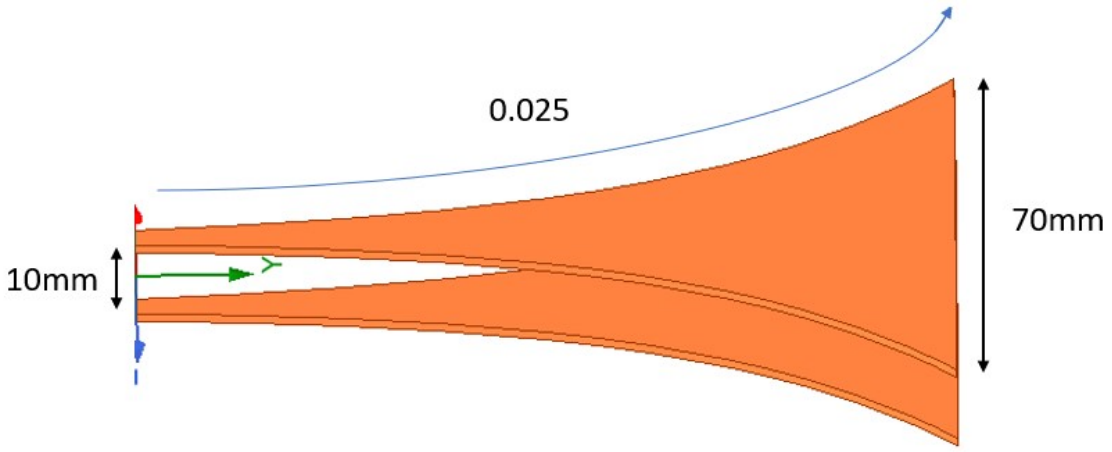

Figure 2.2: Dimension of the testing design

2.1 Theoretical Model

2.1.1 Transmission Line Theory

Lumped Model vs, Distributed Model

Lumped model is the circuit component model which assumes that physical structure of the components do not affect the signal transmission. The current at any point on a wire remain constant. The vol between two terminal does not change. Circuit theory is developed based on this assumption (KVL, KCL). Lumped model is accurate when the physical dimension of the component is less than one tenth of the signal's wavelength.Under this condition, the phase shift between the beginning and the end of the two terminals is negligible. Usually it is the case when the operating frequency is low.

On the other hand, distributed model takes the physical structure of the electronic components into consideration. The voltage and current vary with locations and time instants (Fig.2.3). Distributed model is used when the physical dimension of the electronic component is higher than one-tenth of the signal's wave

length. This is the case of high-frequency circuits or power transmission line.

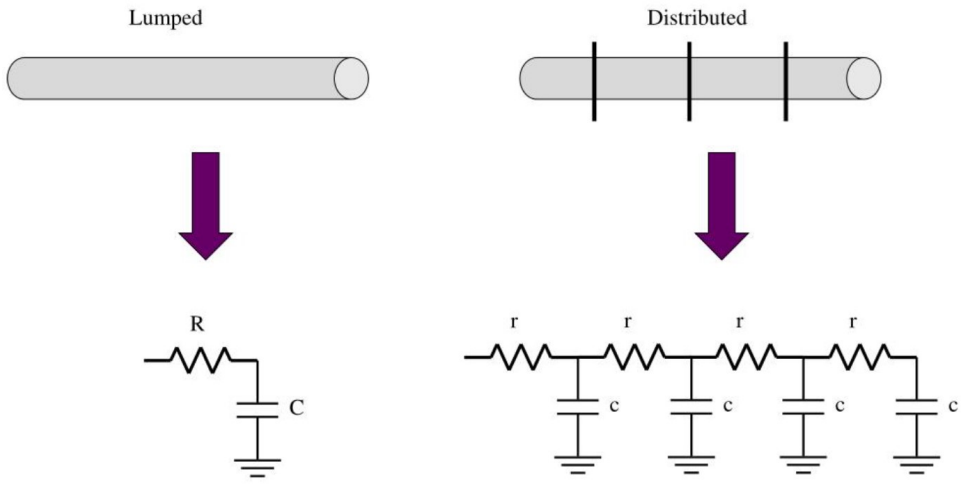

Figure 2.3: Lumped model and Distributed model

The transmission line theory was developed to account for the changes of voltage and current along the wire. The analytical solutions can be derived from circuit theory. The line is sectioned into multiple small sections. The length of each section is small enough so that circuit theory (lumped model) can be applied.

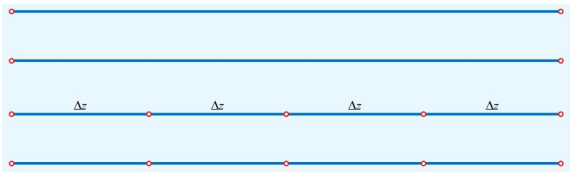

Figure 2.4: Transmission Line with multiple section whose length is Δz

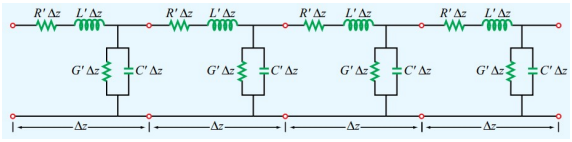

Figure 2.5: The equivalent RLGC model of the transmission line

R' is the resistance per unit length (Ω/m) of the conductors. L' represents the inductance per unit length (H/m) of the two conductor of the small section Δz. C' represents the capacitance per unit length (F/m) between the two conductors. G'

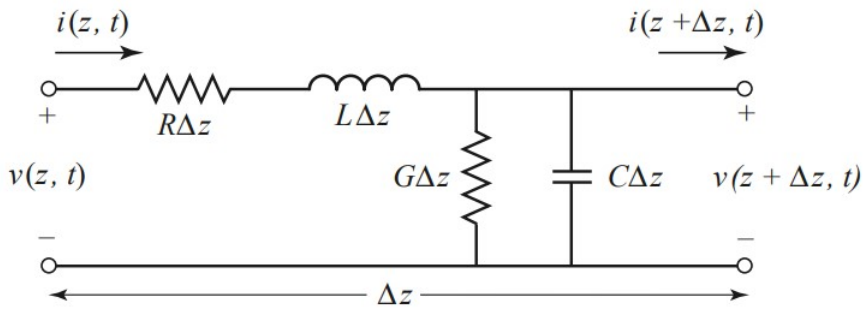

Figure 2.6: Circuit Theory applied to a small section Δz

is the conductance per unit length (S/m) of the medium between the two conductors (Fig. 2.5).

In Fig.2.6, Kirchhoff's voltage law (KVL) and Kirchhoff's current law (KCL) are applied and result in Eq.2.1.1. After that, dividing those two equations with Δz and take the limit as $\Delta z \to 0$ result in Eq.2.1.2. These are Telegraph's equations, the time-domain equations of the transmission line.

$$v(z,t) - R\Delta z i(z,t) - L\Delta z \frac{\partial v(z+\Delta z,t)}{\partial t} - i(z+\Delta z,t) = 0 \qquad (2.1.1a)$$

$$i(z,t) - G\Delta z v(z+\Delta z,t) - C\Delta z \frac{\partial v(z+\Delta z,t)}{\partial t} - i(z+\Delta z,t) = 0 \qquad (2.1.1b)$$

$$\frac{\partial v(z,t)}{\partial z} = -Ri(z,t) - L\frac{\partial i(z,t)}{\partial t} \qquad (2.1.2a)$$

$$\frac{\partial i(z,t)}{\partial z} = -Gv(z,t) - C\frac{\partial v(z,t)}{\partial t} \qquad (2.1.2b)$$

The Telegraph's equations(Eq.2.1.2a) represent the voltage and current along the length of the transmission line at an arbitrary time instant t. In practice, the signal is usually sinusoidal. Thus, with that assumption, Eq.2.1.2 can be simplified to Eq.2.1.3.

$$\frac{\mathrm{d}V(z)}{\mathrm{d}z} = -(R + jwL)I(z) \tag{2.1.3a}$$

$$\frac{\mathrm{d}I(z)}{\mathrm{d}z} = -(G + jwC)V(z) \tag{2.1.3b}$$

From Eq.2.1.3, Eq.2.1.4 can be derived with γ being the complex propagation constant. This variable is a function of frequency (Eq.2.1.5).

$$\frac{\mathrm{d}^2V(z)}{\mathrm{d}z^2} - \gamma^2 V(z) = 0 \tag{2.1.4a}$$

$$\frac{\mathrm{d}^2I(z)}{\mathrm{d}z^2} - \gamma^2 I(z) = 0 \tag{2.1.4b}$$

$$\gamma = \alpha + j\beta = \sqrt{(R + jwL)(G + jwC)} \tag{2.1.5}$$

Above equations are accounted for the losses in general transmission line with the propagation constant γ being complex. Those losses is from the conducting and dielectric loss of the medium between the two conductors. The solution for Eq.2.1.4 can be found as

$$V(z) = V_o^+ e^{-\gamma z} + V_o^- e^{\gamma z} \tag{2.1.6a}$$

$$I(z) = I_o^+ e^{-\gamma z} + I_o^- e^{\gamma z} \tag{2.1.6b}$$

The $e^{-\gamma}$z term describes the wave propagation in +z direction while the $e^{\gamma z}$ represents the wave propagation in -z direction. The real part (α) of the complex propagation constant γ indicates the wave attenuation as it travels through the medium. The imaginary part (β) represents the phase constant of the wave. By solving Eq.2.1.4, we get

$$I(z) = \frac{\gamma}{R + jwL}(V_o^+ e^{-\gamma z} - V_o^- e^{\gamma z}) \tag{2.1.7}$$

or

$$I_o^+ e^{-\gamma z} + I_o^- e^{\gamma z} = \frac{R + jwL}{\gamma} V_o^+ e^{-\gamma z} - \frac{R + jwL^-}{V}{}_o e^{\gamma z} \tag{2.1.8}$$

From Eq.2.1.8, the characteristic impedance of the transmission line Z_o can be defined as

$$Z_o = \frac{R + jwL}{\gamma} = \sqrt{\frac{R + jwL}{G + jwC}} \tag{2.1.9}$$

or

$$Z_o = \frac{V_o^+}{I_o^+} = \frac{-V_o^-}{I_o^-} \tag{2.1.10}$$

In this work, the parallel plate transmission line was used in the modeling process of the sensor. Using Maxwell's equations, the R, L, G and C parameters of the line were derived. In Eq.2.1.11, R_s is the surface resistance of the conductor, w is the width of the plate and h is the distance or separation between the two plates. ϵ, μ and σ are the electrical permittivity, magnetic permeability and electrical conductivity of the medium surrounding the structure, which is soil in this study.

$$R = \frac{2R_s}{w}(\omega/m) \tag{2.1.11a}$$

$$L = \frac{\mu h}{w}(H/m) \tag{2.1.11b}$$

$$G = \frac{\sigma w}{h(S/m)} \tag{2.1.11c}$$

$$C = \frac{\epsilon w}{h}(F/m) \tag{2.1.11d}$$

As shown in Eq.2.1.10, the characteristic impedance Z_o represents the ratio between voltage and current of the line at any particular point along the line. This variable is not a function of frequency but the resistance value of the conductor, the conductance value of the medium, the self-inductance of the conductors and the capacitance between them. If the physical structure of the line is uniform, these

value would remain constant. Thus, so is its characteristic impedance Z_o. The phase constant and phase velocity are

$$\beta = \frac{2\pi}{\lambda} \tag{2.1.12}$$

$$v_p = \frac{\omega}{\beta} = \lambda f \tag{2.1.13}$$

When the incident wave $V_o^+ e^{-\gamma z}$ is generated at the source and propagate along the transmission line, the ratio between it and the current is Z_o. However, if the line is terminated with an arbitrary $Z_L \neq Z_o$, the ratio between voltage and current at the end of the line would be Z_L instead. This mean that a different wave $V_o^- e^{\gamma z}$ with an amplitude so that

$$Z_L == \frac{V_{z=0}}{I_{z=0}} \tag{2.1.14}$$

$$Z_L == \frac{V_o^+ + V_o^-}{V_o^+ - V_o^-} Z_o \tag{2.1.15}$$

With Eq.2.1.15, solving for V_o^-, we have

$$V_o^- = \frac{Z_L - Z_o}{Z_L + Z_o} V_o^+ \tag{2.1.16}$$

The ratio between the reflected wave V_o- and the initial wave V_o^+ is defined as voltage reflection coefficient Γ (Eq.2.1.17).

$$\Gamma = \frac{Z_L - Z_o}{Z_L + Z_o} \tag{2.1.17}$$

$$V(z) = V_o^+ (e^{-j\beta z} + \Gamma e^{j\beta z}) \tag{2.1.18a}$$

$$I(z) = \frac{V_o^+}{Z_o} (e^{-j\beta z} + \Gamma e^{j\beta z}) \tag{2.1.18b}$$

The equation for reflection coefficient Γ represents how much of the wave is reflected back to the source. This parameter is usually expressed in log scale dB. From Eq.2.1.17, the only case in which there is no reflection is when load impedance Z_L is equal to the characteristic impedance Z_o. When it happens, we say that the transmission line is matched. Otherwise, it is unmatched. In practice, it is preferred to have the line matched as it maximizes the power transmission from one end to another. It also prevents potential damage caused by reflected wave to the source. Reflection coefficient is an important figure-of-merit when it comes to determine the efficiency of a structure.

Open-circuit transmission line is a special case in which the load impedance Z_L is infinite. In this case, the reflection coefficient Γ would be one (Eq.2.1.19). It means that all power would be reflected and transmitted back to the source.

$$\Gamma = \lim_{Z_L \to \infty} \frac{Z_L - Z_o}{Z_L + Z_o} = 1 \tag{2.1.19}$$

Short-circuit transmission line is another special case in which the load impedance Z_L is zero. In this case, the reflection coefficient Γ would be also one (Eq.2.1.20). Similarly, all power would be reflected and transmitted back to the source.

$$\Gamma = \frac{Z_L - Z_o}{Z_L + Z_o} = 1 \tag{2.1.20}$$

As discussed above, the structure of the proposed sensor is not uniform. Its width varies exponentially along the path (Fig.1.18). Thus, it is not a uniform transmission line. Transmission line theory can not be used in this case. In order to model the sensor,its structure is divided into multiple small sections. The length of each section is selected to be small enough so that it approached the uniform shape which is rectangular (Fig.2.7).Since each section has uniform shape, transmission line theory can be applied to them. From there, ABCD network was used to cascade all of them to generate the overall result of the entire structure.

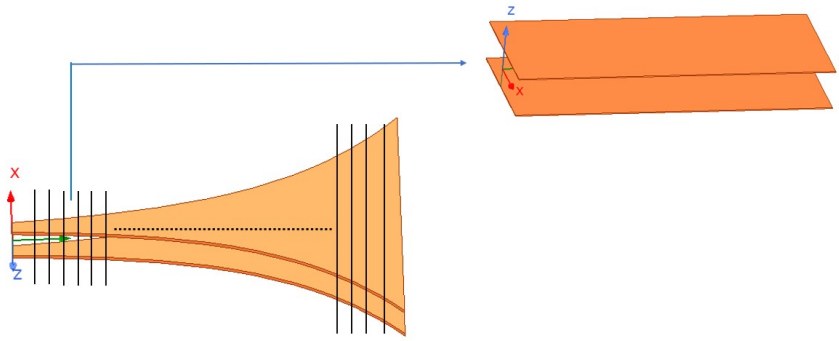

Figure 2.7: Discretization of the proposed sensor structure.

2.1.2 Two-port Network

Two-port network is an electrical circuit with two pairs of terminal connecting to the external circuits. Two-port network is treated as a black box and its properties are presented in a form of matrix. This simplifies the analysis of the system's response to an input from external sources without having to analyze the internal part of the said system [**?**]. The current going into the left side of the port is called I_1. The voltage at two terminal on the left side is called V_1. Similarly, the counterpart of the right terminal is called I_2 and V_2 (Figure 2.8). In this work, we are interested in two type of two-port network: Scattering matrix S-parameter and Transmission Matrix ABCD.

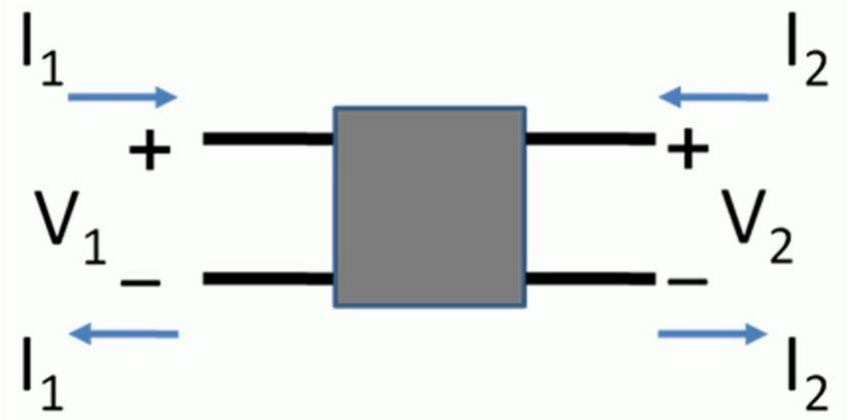

Figure 2.8: General Two-port Network diagram

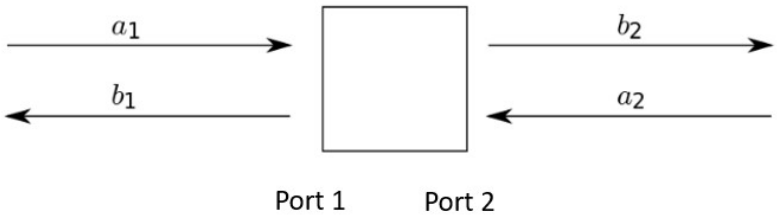

Figure 2.9: S-parameter of two-port network

Scattering matrix S-parameter

In RF circuit, voltage and current are difficult to measure. Their measurement require "open" and "short" condition which are not easy to create with parasitic capacitance and finite inductance at high frequency. Thus, normal two-port networks are not applicable. In these cases, scattering matrix, or S-parameter, is used provide description of the network at its two ports. Instead of measuring voltage or current of the port, S-parameter presents the ration between the voltage waves incident on the ports and those reflected from the ports (Fig.2.9). a_1, b_1 and a_2, b_2 are the incident waves from and reflected waves to port 1 and port 2 respectively. Eq.2.1.21 describe the relationships between them at the two ports [**?**].

$$\begin{bmatrix} b_1 \\ b_2 \end{bmatrix} = \begin{bmatrix} S_{11} & S_{12} \\ S_{21} & S_{22} \end{bmatrix} \begin{bmatrix} a_1 \\ a_2 \end{bmatrix} \tag{2.1.21}$$

As described in Eq.2.1.21, S_{11} is equal to the ratio $\frac{b_1}{a_1}$ with b_1 is the reflected wave at port 1 and a_1 is the incident wave from port 1. This is the figure-of-merit of interest. The wave reflection of the open-circuit transmission line, measured at the source, varies with frequencies. The frequency at which results in the least amount of reflection is the resonant frequencies. It is mainly affected by the electrical length of the transmission line and the surrounding medium. In this study, soil with different moisture level would result in different resonant frequencies. Shift in this measurement is proportional to the changes in water content of soil. In lab setup, S_{11} can be measured directly with vector network analyzer (VNA). However, in

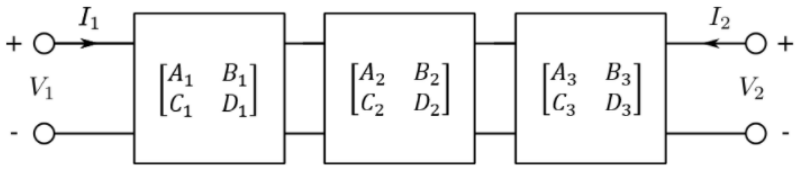

Figure 2.10: Example of cascaded system

theoretical model, given the nonuniform nature of the proposed sensor, transmission matrix ABCD is needed for the calculation.

Transmission Matrix ABCD

ABCD parameter is one type of two-port network. Its other name is forward network. In short, this network describes the relationship between the inputs and the outputs (current and voltage) (Eq.2.1.23) [**?**]. Thus, it simplifies the calculation of the overall system which is made of multiple cascaded small sub-system.

$$\begin{bmatrix} V_1 \\ I_1 \end{bmatrix} = \begin{bmatrix} A & B \\ C & D \end{bmatrix} \begin{bmatrix} V_2 \\ I_2 \end{bmatrix} \tag{2.1.22}$$

$$\begin{aligned} V_1 &= AV_2 + BI_2 \\ I_1 &= CV_2 + DI_{2]} \end{aligned} \tag{2.1.23}$$

If multiple networks are connected to each other, the overall ABCD parameter of the total network is the multiplication of all subsections [**?**]. As seen in Fig.2.10, there are three sub-systems being connected to each other. Each subsystem has its own ABCD parameter, label as [1], [2] and [3] respectively. The ABCD parameter of the overall system can be calculated by multiplying the ABCD parameter of each sub-system (Eq.2.1.24).

$$\begin{bmatrix} V_2 \\ I_2 \end{bmatrix} = \begin{bmatrix} A_1 & B_1 \\ C_1 & D_1 \end{bmatrix} \begin{bmatrix} A_2 & B_2 \\ C_2 & D_2 \end{bmatrix} \begin{bmatrix} A_3 & B_3 \\ C_3 & D_3 \end{bmatrix} \begin{bmatrix} V_1 \\ I_1 \end{bmatrix} \tag{2.1.24}$$

In this work, the sensor structure is discretized into small sections. The length of each section is small enough so that changes in its width approaches zero which is rectangular shape (Fig.2.7). The ABCD parameter of each section can then be found with Eq.2.1.25. Z_o and γ are the transmission line parameters and can be calculated with Eq.2.1.9 and Eq.2.1.5. After calculating the ABCD matrix of each section, the ABCD parameter of ther overall structure is determined by cascading all the sub-section with Eq.2.1.24. After that, the S_{11} value of the sensor is calculated with Eq.2.1.26.

$$A = cosh(\lambda l) \tag{2.1.25a}$$

$$B = Z_o sinh(\gamma l) \tag{2.1.25b}$$

$$C = \frac{sinh(l)}{Z_o} \tag{2.1.25c}$$

$$D = cosh(\gamma l) \tag{2.1.25d}$$

$$S_{11} = \frac{A + B/Z_o - CZ_o - D}{A + B/Z_o + CZ_o + D} \tag{2.1.26}$$

2.2 Simulating Model in HFSS

HFSS is a commercial numerical solver developed by Ansys. It was introduced in 1980s and has become the gold-standard in the industry since then. HFSS uses the nummerical technique called Finite Element Method in which the model is divided into many smaller subsections called finite elements. The electromagnetic fields, not voltage nor current, is solved directly with Maxwell equations through an iterative process. At the beginning, HFSS generates an initial mesh and calculate the EM field generated by a source at predefined frequency range. HFSS is then determines the regions in which the solution has a high degree of error and refine it. The mesh at those region gets divided into smaller section. The solver then com-

pute another solution and compare it with the previous one. If the error is within a predefined number then the process stops. Otherwise the same steps would be repeated (Fig.2.11) [**?**].

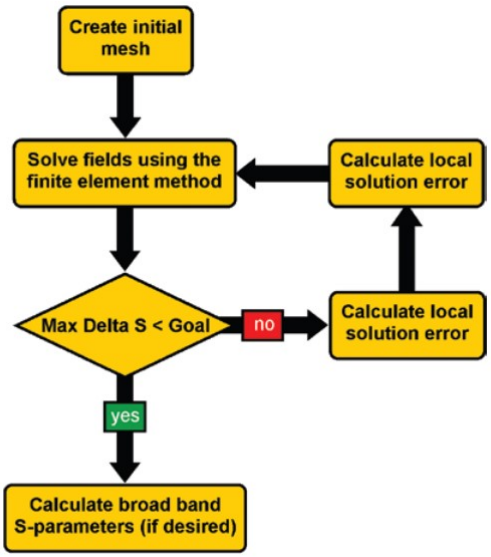

Figure 2.11: Flowchart of HFSS's iterative process

The proposed sensor model was built in the High-frequency Structure Simulator (HFSS) software. The model consists of two copper plate, separated by a certain distance and connected by a small metal sheet acting as a source. The source is assumed to be perfect. Its impedance is set to be 50Ω. The solver setting is set to be default. The sensor is 120mm and the boundary layer shifting between the 10-mm and 100-mm marks of the sensor with increment of 10mm (Fig.2.12). The simulation starts with the boundary layer at the beginning and moving deeper toward the end of the sensor There are three scenarios.

2.3 Result

Fig.2.13, Fig.2.14 and Fig.2.15 have resonant frequencies of proposed sensor design at different boundary layer depths across three cases. . There are about 50 to 100MHz discrepancy between the two. This is the result of fringing effect. Upon charged, the medium between the two metal plate is not the electric field generated.

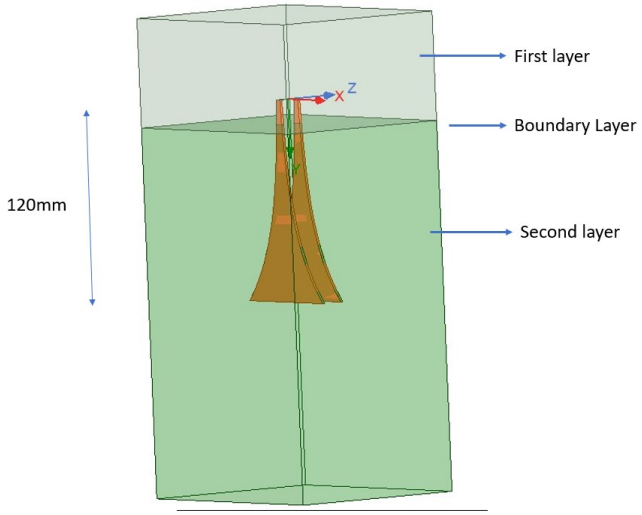

Figure 2.12: Proposed sensor modeled in HFSS

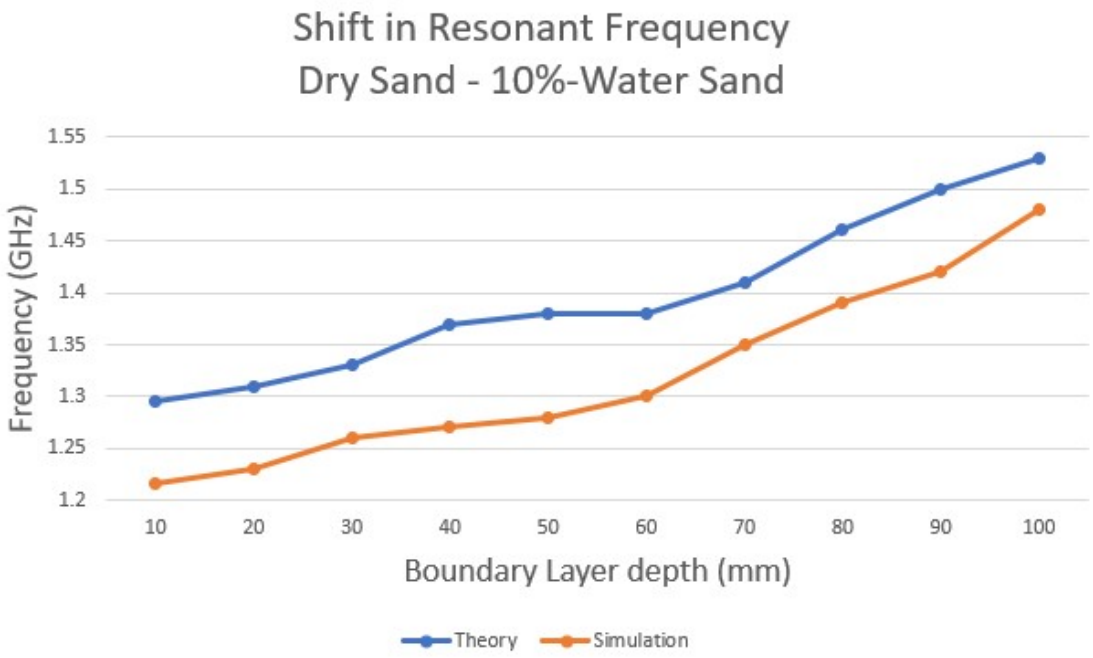

Figure 2.13: Case 1 - Resonant frequencies of the proposed soil sensor at different boundary layer

The atom polarization also happen in some distance away, not just strictly between the surface area of the two plate (Fig.2.16). Thus, the actual capacitance is effective higher than the one obtained from Eq. As a result, the resonant frequencies would be lower, or shifted to the left, as shown in Fig.2.13.

The result of theoretical and simulating model share a similar upward trend as the boundary layer shifted downward. This is within expectation. As moisture

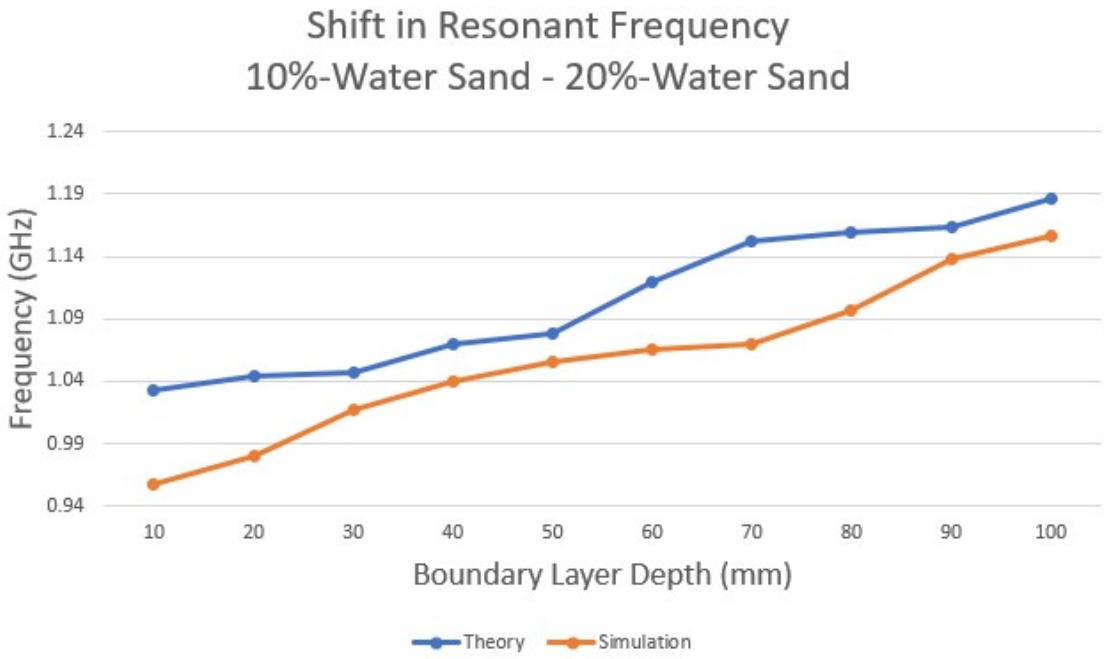

Figure 2.14: Case 2 - Resonant frequencies of the proposed soil sensor at different boundary layer

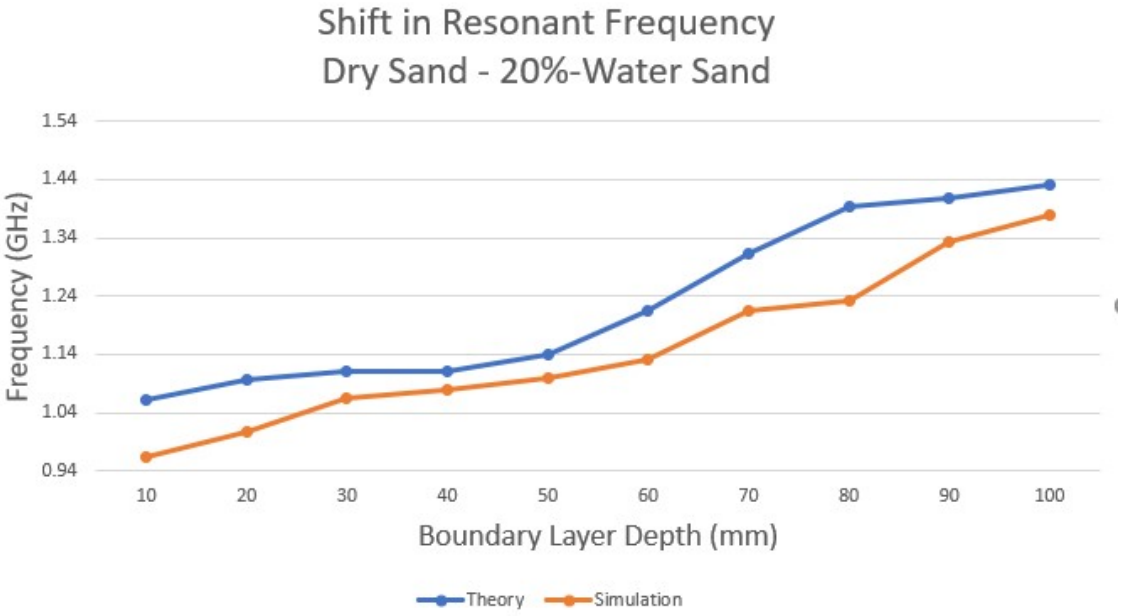

Figure 2.15: Case 3 - Resonant frequencies of the proposed soil sensor at different boundary layer

level increase, so does the dielectric constant value of the soil which is proportional to the capacitive effect of the medium. Thus, the resonant frequency is expected to be shifted to the lower band as water content of the soil increases. Since the first layer is set to be the drier than the second one and the boundary layer moved downward,

the effective dielectric value of the overall system is lowered. This resulted in lower capacitive effect and shifting the resonant frequencies to higher band. Another observation from these results is that the frequency shifting when the boundary change at the end of the sensor is higher than the changes in the middle. This is the case for all three soil scenarios.

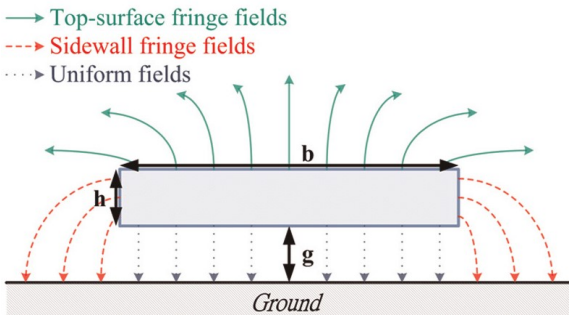

Figure 2.16: Fringing Effect of Capacitor

As shown the above figures, the proposed sensor design is able to capture changes in soil layers with measurement in resonant frequency. However, rectangular-shape sensor would be able to capture these changes as well. In the next chapter, measurement for the proposed sensor with exponential shape and conventional sensor with rectangular shape would be done in the lab for performance comparison. Their setup would be modeled in HFSS to compare the result.

Chapter 3

Performance Analysis

The proposed sensor was designed to encode the depth information in its physical structure. For this purpose, the width of the sensor is designed to vary exponentially. This design allows for more changes in capacitance between the two metal patches of the sensor as the boundary between layers shifts. This would results in higher frequency shifting in S11 measurement.

The performance of the exponential-shape sensor was studied and compared with the standard rectangular-shaped one. The two sensors were fabricated and the measurement setup were arranged in the lab. Sand was used as the testing medium. Two scenarios were tested: Air and dry sand, dry sand and 20%-water sand.

3.1 Setup

3.1.1 Measurement in the lab

Instead of using metal plate, the sensor was fabricated as copper trace on a printed circuit board (PCB). The substrate is FR4. It is made of epoxy fiberglass laminate sheet. The trace was coated to prevent the copper from being oxidized (Fig.3.1. The two PCB was soldered to a board connector. At the end of the line, SMA connector was used to connect with the FieldFox VNA through a coaxial cable (Fig.3.2). The soil was contained in a 13mm x 19mm x 13mm plastic box. The boundary between the two layers moved from 30mm to 105mm with 15mm increment (Fig.3.3.

Figure 3.1: Sensor before and after surface coating

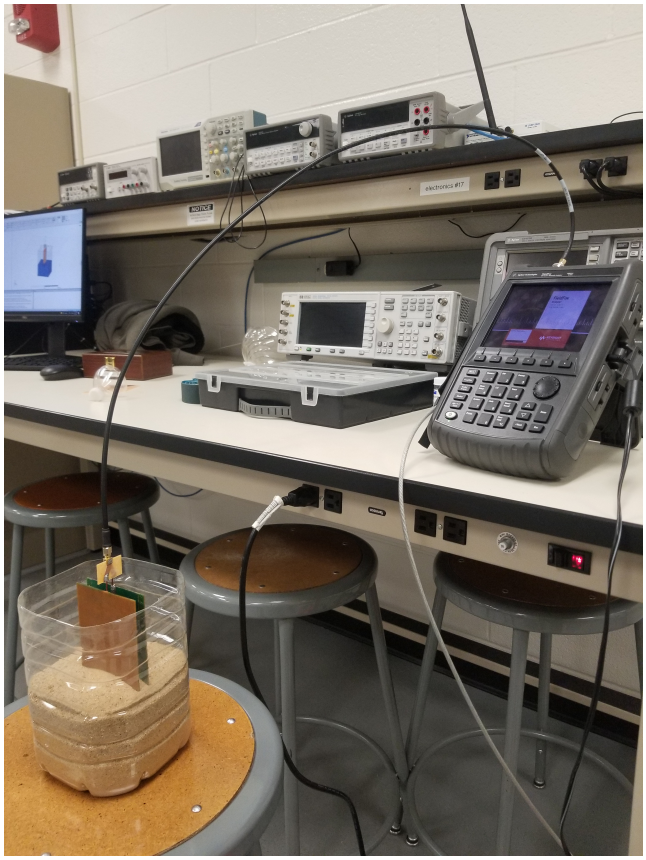

Figure 3.2: Measurement setup with plastic container and sensor on PCB

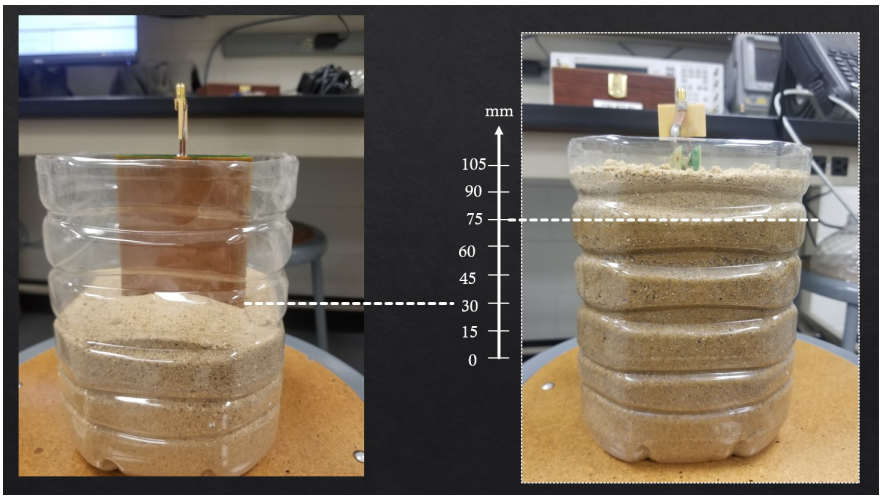

Figure 3.3: Boundary Layer increment (Air and Dry sand, Dry sand and Wet sand)

To create the medium (sand) whose water content was 20%, the direct method was employed. The dry sand was weighed initially and the amount of needed water was calculated. The water was then carefully obtained with measuring cup and slowly poured over the dry sand (Fig.3.4). After that, we waited 10 minutes for the water to settle in before adding the dry-sand layer on top of it. This process was repeated for different layer's depth.

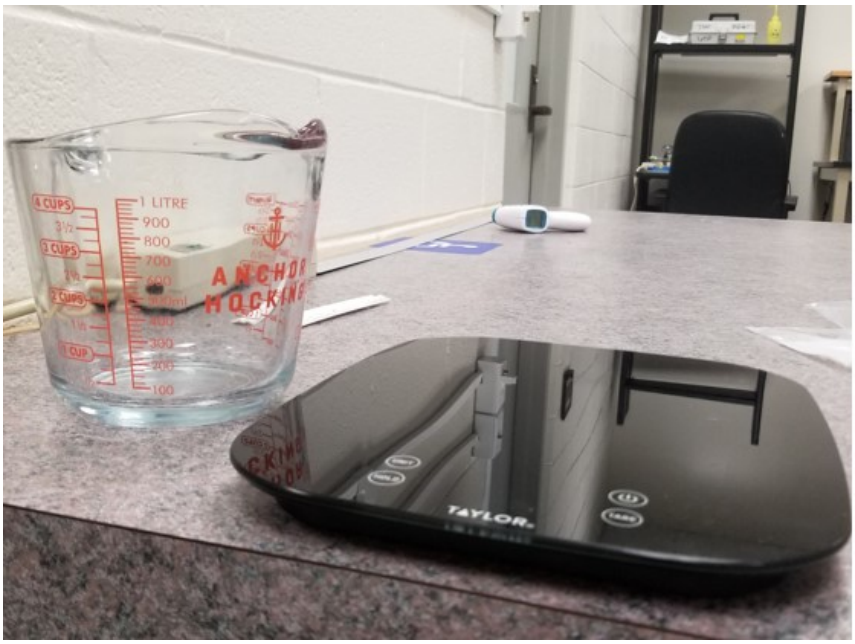

Figure 3.4: Measuring cup and scale

3.1.2 In the simulation environment HFSS

The setup in the lab was carefully modeled in the simulation software. The board connector, soil container as well as wire were recreated in HFSS so that the result could be close to the real measurement as much as possible. The only difference between the two is that in simulation, the SMA connector was not present. This component was created separately before. However, this model was not created accurately as it failed the running test. Thus, SMA connector was omitted in the simulation setup (Fig.3.5). Similar process was done for the rectangular-shaped sensor (Fig.3.6).

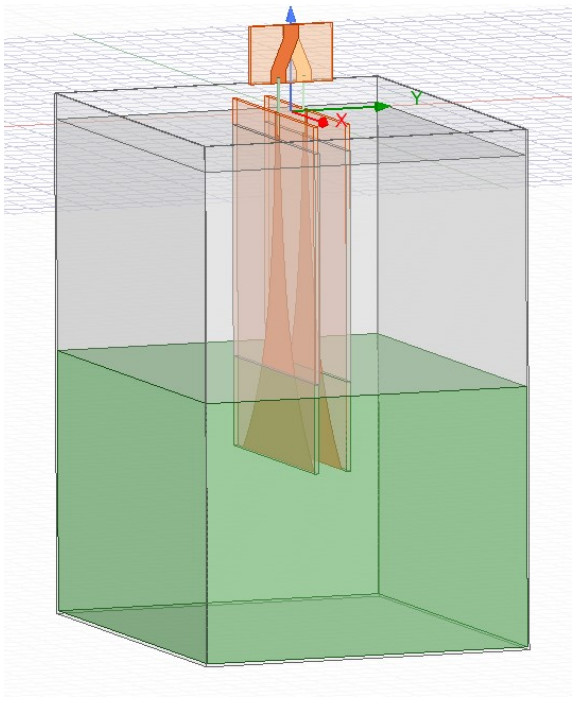

Figure 3.5: Simulation setup for exponential-shaped sensor in HFSS

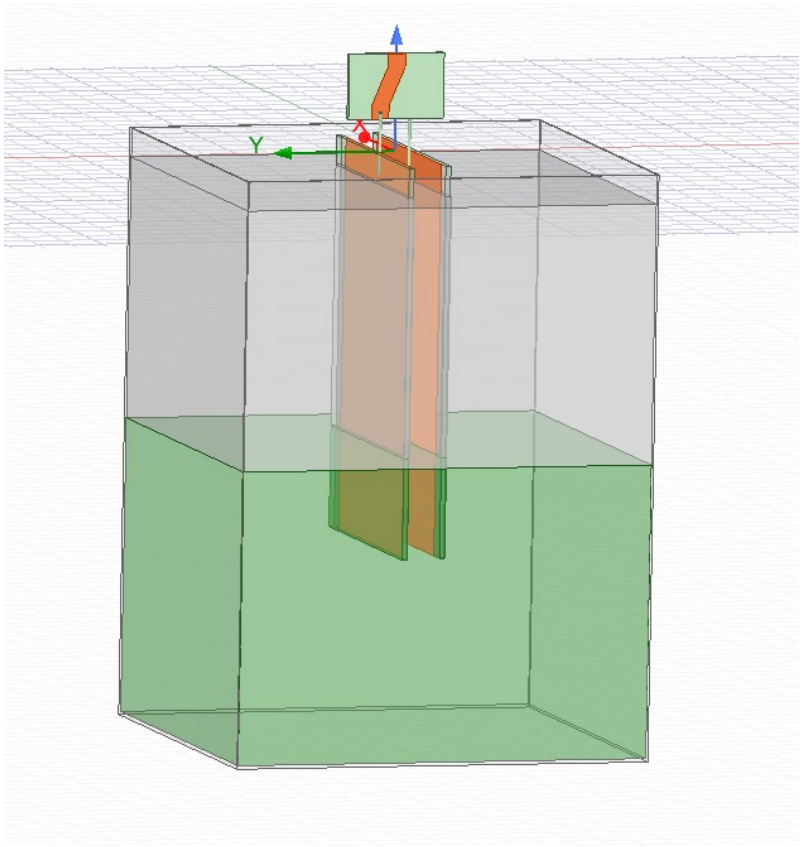

Figure 3.6: Simulation setup for rectangular-shaped sensor in HFSS

3.2 Result

3.2.1 Dry Sand - Air

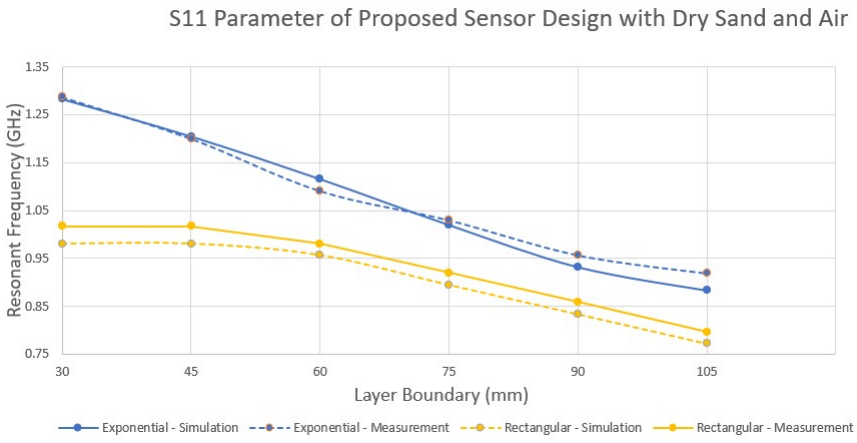

Figure 3.7: S11 Measurement of Exponential and Rectangular sensor with Dry Sand and Air

In Fig.3.7, the S11 measurement of the proposed sensor design, exponential shape, and the standard on with rectangular shape were plotted together. The two layers were dry sand and air. The boundary between them vary from 30mm to 105mm. As seen in that figure, there are around 50MHz discrepancies between the simulation and the experiment. This difference stay consistent through out the experiments. The changes in resonant frequencies as the boundary of the two medium shifted is similar between the simulation and the experiment. The sensitivity of the exponential-shape sensor is observed to be higher than the rectangular-shaped one as the boundary layer changing from 30mm to 60mm. This agrees with the observation in the previous chapter as it is where the width of the sensor varies the most.

The sensitivity of the two design coincides as the boundary changing from 60mm to 90mm. This make senses as this is where the width of the exponential shape vary least. When the width of the two sensors has the same variation, the changes it captured are similar.

3.2.2 20%-Water Sand - Dry Sand

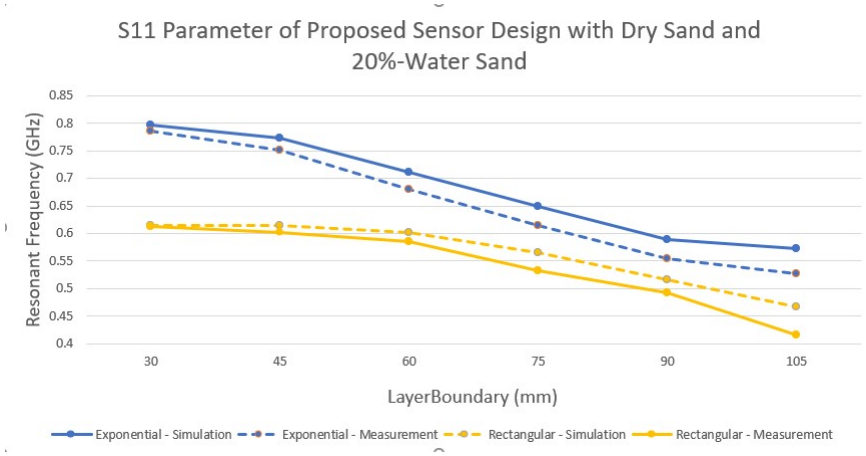

Figure 3.8: S11 Measurement of Exponential and Rectangular-shape design with 20%-Water Sand and Dry Sand

Fig.3.8 has the results of the two sensor designs placed in the contained with wet and dry sand. The lab measurements and simulation's were plotted together for

comparison. Similar to the case of air and dry sand, the boundary between the two mediums varied from 30mm to 90mm. Observation made for Fig.3.7 agrees with the previous case. The sensitivity of the exponential-shape design is greater than the rectangular one when the boundary changes from 30mm to 60mm. As the changes in the width of the exponential-shaped sensor getting smaller, it captured as much changes in soil medium as the rectangular-shaped one. One noticeable difference in this case is that as the soil moisture increased, the discrepancies between the lab measurement and the simulated results became higher. This could be due to that fact that the water water were not accurately measured, obtained or added.

Chapter 4

Parametric Analysis

4.1 Design goal

The objective of this study is designing a sensor capable of sensing soil's continuous moisture profile at root zone, which is around 500mm. After confirming the proposed design's capability of capturing more changes in soil layers compared to standard one, the effect of the sensor's design parameter such as separation, end-width and curvature constant were carried out. Given the limitation of lab measurement, this study was done only in simulation software HFSS.

4.2 Simulation setup

In this setup, the sensor was built as metal plates instead of copper traces on PCB. This was aimed to model the potential real-life structure it is not practical to use 500-mm PCB. Similarly to other simulations in previous chapter, the source connected the two metal plates was assumed to be perfect and did not add any effect to the result. The sensor was set to be placed completely within the soil medium. The surrounding medium is assumed to be air. The nominal design is 500mm long with 200-mm end-width . The separation between the two plates are 90mm. The curvature constant is 0.008. As observed in previous chapter, more changes is captured by the proposed design when the boundary layer shifted at the end of the sensor. This result is within the expectation as the width of the sensor varies the most toward the end. To verify this assessment, for the parametric study of the curvature constant, two cases of boundary shifting were evaluated: in the middle of the sensor and toward the end of the sensor.

Three cases of soil were tested (dry sand and 10%-water sand, 10%-water sand and 20%-water sand, dry sand 20%-water sand). Three parameters, separation, width and curvature shape were varied around the nominal design. (Fig.4.1 and Fig.4.2).

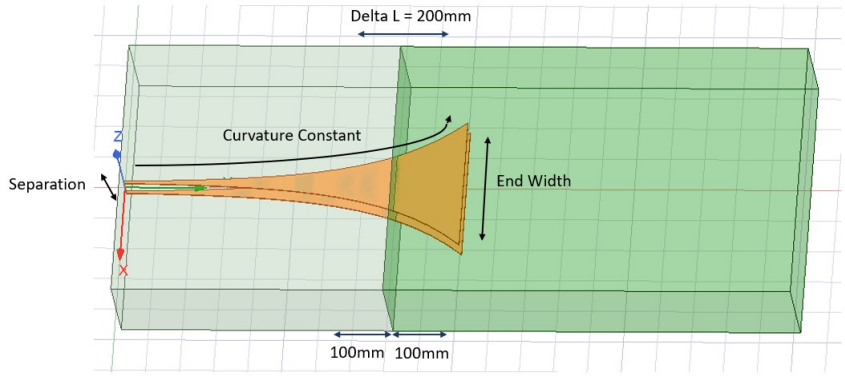

Figure 4.2: Simulation setup in HFSS with boundary varying at the end of the sensor

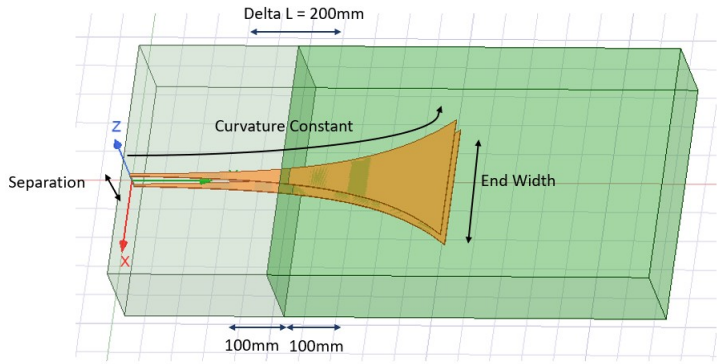

Figure 4.1: Simulation setup in HFSS with boundary varying in the middle of the sensor

When the simulation finished, the resonant frequency of each cases was recorded. The sensitivity of the sensor with respect to the design parameter is the figure-of-merit in interest. It was calculated by finding the the slope between the shift in resonant frequencies and the boundary changes of each design variation.

4.3 Result

4.3.1 Plate's Separation

As seen in Fig.4.3, as the two metal plates getting further, the sensitivity of the sensor became smaller in all three cases. This observation agreed with the

Electromagnetic theory. As the capacitive effect depends on the medium between the two conductors, the further they are apart, the effect the medium has on them. On the side note, most changes in resonant frequencies happened when the two medium in the soil were dry sand and 20%-water sand, followed by the case of dry sand and 10%-water sand. This aligns with the expectation as the difference between the two mediums are highest in these two scenarios.

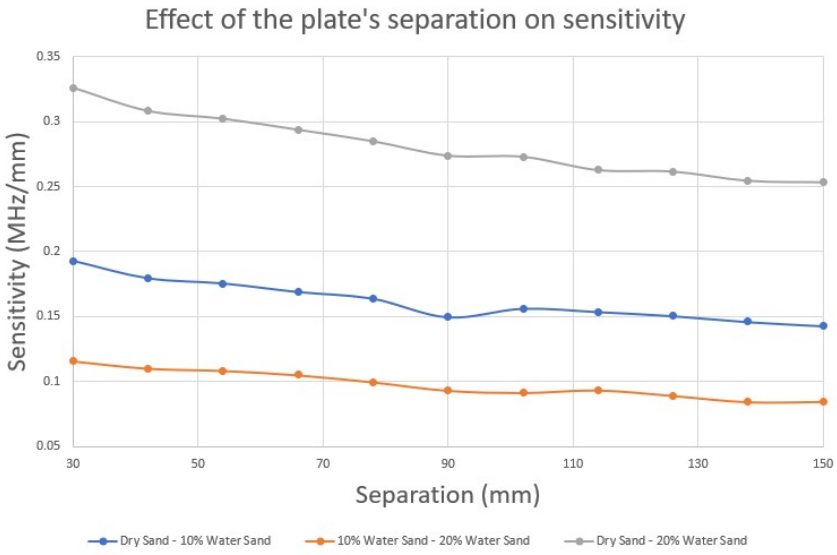

Figure 4.3: Sensitivity of the sensor at different separations

4.3.2 End-width

The end-width is the width of the sensor at the end of its length. It partly dictates how fast the sensor's width varies. The sensitivity of the sensor at different end-widths is plotted in the Fig.4.4. As observed in that figure, the sensor is the most sensitive when the width is largest. Similarly, highest sensitivity was observed in the case of dry sand and 20%-water sand while the lowest happened in the case of 10%-water sand and 20%-water sand. This is the expected result as difference between case#3 is less than the other two cases.

Figure 4.4: Sensitivity of the sensor at different end-widths

4.3.3 Curvature constant

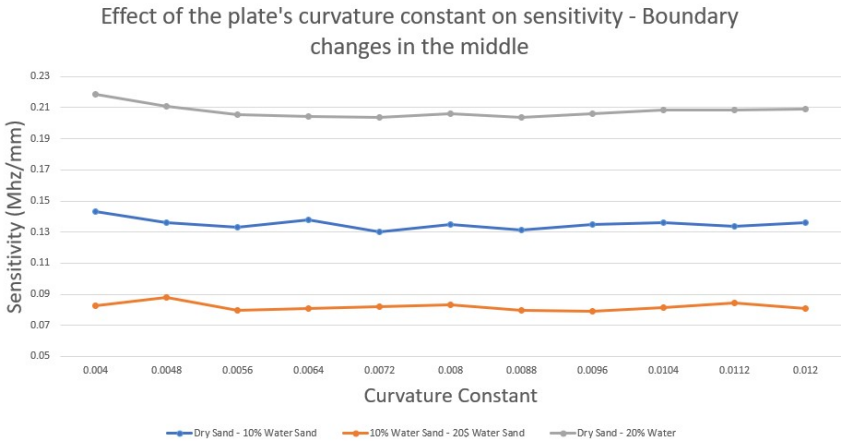

Figure 4.5: Sensitivity of the sensor at different end-widths (boundary varied in the middle)

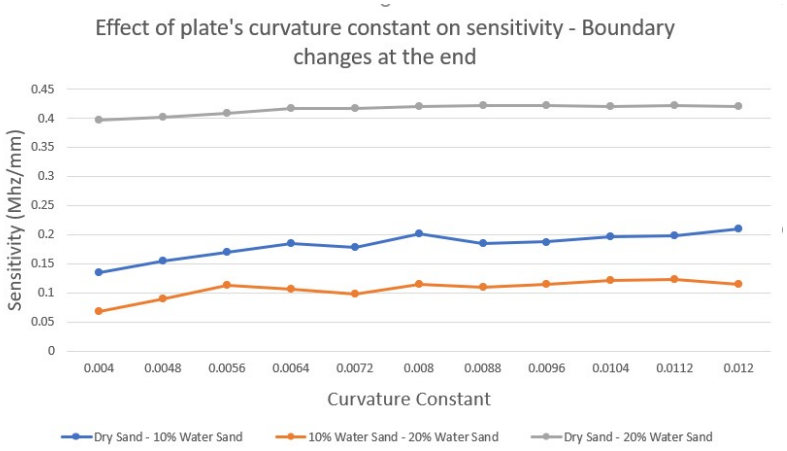

Figure 4.6: Sensitivity of the sensor at different end-widths (boundary varied at the end)

As observed in Fig.4.5, when the boundary layers shifting in the middle of the sensor, changes in curvature constant does not contribute much to the result. In all three soil scenarios, the shift in resonant frequency appears to be minimal. On the other hand, as shown in Fig.4.6, sensor with higher curvature constant is more sensitive to the changes in boundary layers toward the end of the sensor.

4.3.4 Summary

The result from the parametric study show that the optimized design should have the distance between the two plate as small as possible. However, this should be done properly to avoid short-circuit issue. For end-width, the wider it is, the more sensitive the sensor become. However, it might not be practical to have a big sensor as it would be difficult to transport and assemble. Regarding the curvature constant, it was observed that the sensor has better performance with high curvature constant when the boundary layer changes at the end of the sensor. This is due to the fact that the sensor's width vary the most in this location. Thus, for sensor design, the curvature constant value depends on the application. For the boundary layer sensing purpose at a narrow depth, it is better to have a high value of this parameter. However, if the sensor is designed to have a bigger profile sensing depth, it would be preferable to have the curvature constant small. Though the trade-off

would be lower sensing resolution.

Chapter 5

Conclusion and Future work

5.1 Conclusion

In this study, we present a novel sensor for continuous soil's moisture profile. The depth information is encoded into the sensor's physical shape. The design is based on the capacitance approach which determines the water content of soil through the shifts in resonant frequencies.

Theoretical and simulating model of the sensor design were developed. Their result agreed that the proposed design is capable of capturing changes of boundary layers in soil. Experimental result in the lab concluded that the proposed sensor design has higher performance than the regular design when the boundary changes happen toward the end of the probe at which sensor's width varies the most. A parametric study was carried out and validated this observation.

5.2 Future Work

The new sensor design for soil's moisture profile is shown to be able to measure changes in soil layers. It is more sensitive to boundary shifting in soil compared to the conventional design toward the end of the sensor.

In this study, we focused on the validating the capability of the proposed sensor design and how its performance is affected by the design parameters. While the result verified the capability of the new design, it is only at a certain part of the sensor. In future work, we will work on an improved design which could perform continuous soil's moisture profile, not just a certain part, but along the entire sensor's length. In addition, we will carry out experimental measurement for more real data. This will be then used in the working of the inversion and calibration process.

Bibliography

[1] B. Kashyap and R. Kumar, "Sensing methodologies in agriculture for soil moisture and nutrient monitoring," *IEEE Access*, vol. 9, pp. 14 095–14 121, 2021.

[2] S. B. Jones, J. M. Wraith, and D. Or, "Time domain reflectometry measurement principles and applications," *Hydrological processes*, vol. 16, no. 1, pp. 141–153, 2002.

[3] V. P. Drnevich, C.-P. Lin, Q. Yi, and J. E. Lovell, "Real-time determination of soil type, water content, and density using electromagnetics," 2001.

[4] X. Yu, N. Zhang, A. Pradhan, B. Thapa, and S. Tjuatja, "Design and evaluation of a thermo-tdr probe for geothermal applications," *Geotechnical Testing Journal*, vol. 38, no. 6, pp. 864–877, 2015.

[5] B. Will and I. Rolfes, "Comparative study of moisture measurements by time domain transmissometry," in *SENSORS, 2013 IEEE.* IEEE, 2013, pp. 1–4.

[6] J. Hrisko, "Capacitive soil moisture sensor theory, calibration, and testing," *no*, vol. 2, pp. 1–12, 2020.

[7] L. Yu, W. Gao, R. R. Shamshiri, S. Tao, Y. Ren, Y. Zhang, and G. Su, "Review of research progress on soil moisture sensor technology," *International Journal of Agricultural and Biological Engineering*, vol. 14, no. 4, pp. 32–42, 2021.

[8] J. Cihlar and F. T. Ulaby, "Dielectric properties of soils as a function of moisture content," Tech. Rep., 1974.

[9] M. Thalheimer, "A low-cost electronic tensiometer system for continuous monitoring of soil water potential," *Journal of Agricultural Engineering*, vol. 44, no. 3, pp. e16–e16, 2013.

[10] G. S. Campbell, "Soil water potential measurement: An overview," *Irrigation Science*, vol. 9, no. 4, pp. 265–273, 1988.

[11] P. C. Dias, W. Roque, E. C. Ferreira, and J. A. S. Dias, "A high sensitivity single-probe heat pulse soil moisture sensor based on a single npn junction transistor," *Computers and electronics in agriculture*, vol. 96, pp. 139–147, 2013.

[12] M. B. de Morais França, F. J. Morais, P. Carvalhaes-Dias, L. C. Duarte, and J. A. S. Dias, "A multiprobe heat pulse sensor for soil moisture measurement based on pcb technology," *IEEE Transactions on Instrumentation and Measurement*, vol. 68, no. 2, pp. 606–613, 2018.

[13] D. Chanasyk and M. A. Naeth, "Field measurement of soil moisture using neutron probes," *Canadian Journal of Soil Science*, vol. 76, no. 3, pp. 317–323, 1996.

[14] F. T. Ulaby, E. Michielssen, and U. Ravaioli, *Fundamentals of applied electromagnetics*. Pearson Upper Saddle River, NJ, 2015, vol. 7.

[15] G. C. Topp, J. Davis, and A. P. Annan, "Electromagnetic determination of soil water content: Measurements in coaxial transmission lines," *Water resources research*, vol. 16, no. 3, pp. 574–582, 1980.

[16] W. Skierucha and A. Wilczek, "A fdr sensor for measuring complex soil dielectric permittivity in the 10–500 mhz frequency range," *Sensors*, vol. 10, no. 4, pp. 3314–3329, 2010.

[17] Y. Kojima, R. Shigeta, N. Miyamoto, Y. Shirahama, K. Nishioka, M. Mizoguchi, and Y. Kawahara, "Low-cost soil moisture profile probe using thin-film capacitors and a capacitive touch sensor," *Sensors*, vol. 16, no. 8, p. 1292, 2016.

[18] Z. Gao, Y. Zhu, C. Liu, H. Qian, W. Cao, and J. Ni, "Design and test of a soil profile moisture sensor based on sensitive soil layers," *Sensors*, vol. 18, no. 5, p. 1648, 2018.